Performance Analysis of Multiband OFDM UWB Communications With Application to Range Improvement

Qiyue Zou, *Student Member, IEEE*, Alireza Tarighat, *Member, IEEE*, and Ali H. Sayed, *Fellow, IEEE*

***Abstract*—Ultrawideband (UWB) radio is a promising solution for high-rate wireless communications over short ranges. In this paper, the performance of multiband orthogonal frequency-division multiplexing (MB-OFDM) UWB systems is analyzed using the Saleh–Valenzuela channel model in terms of the packet error rate and the transmission range for indoor environments. The performance improvements resulting from the use of linear precoding and multiple antenna techniques are also analyzed and compared. It is shown both by theory and computer simulations that the two methods can effectively enlarge the transmission range of UWB devices.**

***Index Terms*—Bit error rate (BER), linear precoding, multiple antennas, orthogonal frequency-division multiplexing (OFDM), packet error rate (PER), performance analysis, range improvement, Saleh–Valenzuela (S–V) channel model, ultrawideband (UWB).**

I. Introduction

ULTRAWIDEBAND (UWB) communication technology is emerging as a leading standard for high-data-rate applications over wireless networks [2]–[4]. Due to its use of a high-frequency bandwidth, UWB can achieve very high data rates over the wireless connections of multiple devices at a low transmission power level close to the noise floor. The interest in UWB systems has been sparked by an order issued by the Federal Communications Commission (FCC) in February 2002 [5]. In this order, the FCC allocated the spectrum from 3.1 to 10.6 GHz for unlicensed use by UWB transmitters operated at a limited transmission power of -41.25 dBm/MHz or less. Since the power level allowed for UWB transmissions is considerably low, UWB devices will not cause significantly harmful interference to other communication standards. Given the heightened interest in UWB technology following the FCC's order, the IEEE 802.15.3a High Rate Alternative Physical Layer (PHY) Task Group (TG3a) for Wireless Personal Area Networks (WPAN) has been established to standardize the development of UWB devices. Different proposals for the PHY are under consideration by the working group [6]. The orthogonal frequency-division multiplexing (OFDM)-based physical layer is one of the most promising options for the PHY due to its capability to capture multipath energy and eliminate intersymbol interference [7]. Our focus in this paper will be on the OFDM-based modulation scheme for UWB communications.

Despite the aforementioned merits, the extremely short range, e.g., 10 m for a data rate of 110 Mb/s, puts UWB at an obvious disadvantage when compared to other competitive technologies, such as the soon coming IEEE 802.11n standard, which supports a data rate of 200 Mb/s for 40 m in indoor environments. Hence, to push UWB as an attractive option for WPAN and other applications, it is crucial to improve the range limit of UWB devices. We shall do so as follows: First, we analyze the theoretical performance of the multiband OFDM (MB-OFDM) scheme that is proposed by the IEEE 802.15.3a working group for UWB communications [8]. The analysis shows that the bit-interleaved convolutional coded scheme can achieve a coding gain to combat fading. Using the Saleh–Valenzuela (S–V) model, we can also establish that there is a significantly rich spectral diversity in the ultrawide bandwidth that can be exploited to improve the performance. Motivated by these observations, the linear precoding [9] and multiple antenna [10] techniques can be applied to the MB-OFDM scheme to improve the transmission range. Linear precoding "spreads" each transmitted symbol into several independent subcarriers to improve the transmission reliability, whereas multiple transmit and receive antennas achieve a diversity gain to improve the transmission range. For example, it will be seen that with two transmit and two receive antennas, the transmission range can be enlarged from 10 m to more than 30 m for the data rate of 110 Mb/s. Although linear precoding and multiple-input–multiple-output (MIMO) OFDM techniques are known in the literature for improving the reliability of wireless communications, this paper focuses on the following aspects: First, we provide an analysis of MB-OFDM UWB systems with channel coding in the presence of an experimental UWB channel model. The analysis leads to results on the uncoded bit error rate (BER), coded BER, and packet error rate (PER) as a function of the signal-to-noise ratio (SNR) and range and takes into account a practical link budget. This analysis is helpful in validating the many simulation results (without

Manuscript received January 22, 2006; revised October 20, 2006, February 27, 2007, and March 6, 2007. This work was supported in part by the National Science Foundation under Grant ECS-0401188 and Grant ECS-0601266. This paper was presented in part at the IEEE International Conference on Acoustics, Speech, and Signal Processing, Toulouse, France, May 2006 [1]. The review of this paper was coordinated by Prof. Y. Ma.

Q. Zou and A. H. Sayed are with the Department of Electrical Engineering, University of California, Los Angeles, CA 90095 USA (e-mail: eqyzou@ee.ucla.edu; sayed@ee.ucla.edu).

A. Tarighat was with the Department of Electrical Engineering, University of California, Los Angeles, CA 90095 USA. He is now with WiLinx, Los Angeles, CA 90025 USA (e-mail: tarighat@ee.ucla.edu).

Color versions of one or more of the figures in this paper are available online at http://ieeexplore.ieee.org.

Digital Object Identifier 10.1109/TVT.2007.901957

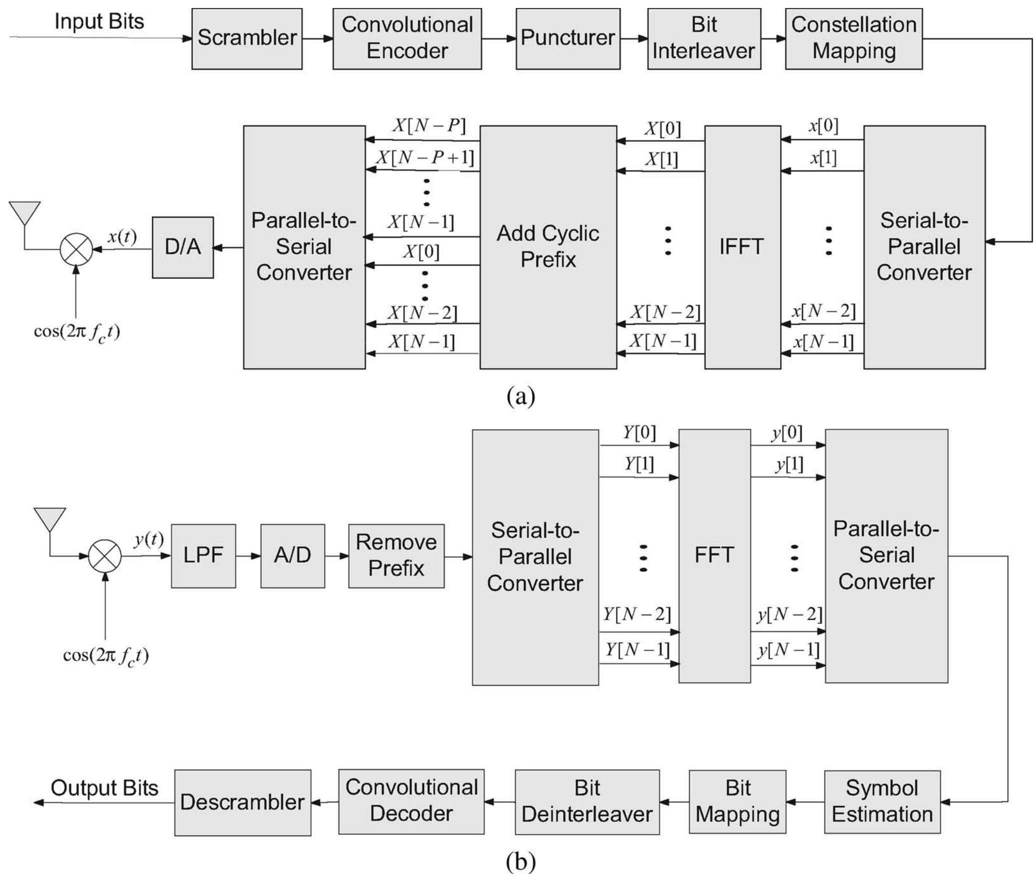

Fig. 1. Block diagrams of the transmitter and receiver of an MB-OFDM system. (a) Transmitter. (b) Receiver.

any analysis) provided for the MB-OFDM UWB system by the industry and UWB standardization community. Second, a critical limitation in UWB systems is their relatively short range. This paper presents an analysis on the achievable range improvement by using precoding and MIMO techniques.

This paper is organized as follows: Section II gives a brief review of the MB-OFDM modulation scheme. The analytical results on the coded BER and link PER of MB UWB systems are presented in Section III. Section IV illustrates how the linear precoding and multiple antenna techniques can be exploited and also analyzes their performance. The simulation results are presented in Section V, and the conclusions are given in Section VI.

II. MB-OFDM UWB Systems

In an MB-OFDM UWB system, the spectrum is divided into several subbands, with a bandwidth of 528 MHz each [7]. The system operates in one subband and then switches to another subband after a short time. In each subband, OFDM modulation is used to transmit data symbols. The transmitted symbols are time interleaved across the subbands to utilize the spectral diversity to improve the transmission reliability.

The fundamental transmitter and receiver structure of an MB-OFDM system is illustrated in Fig. 1. At the transmitter, the bits from information sources are first whitened by the scrambler and then encoded by the convolutional encoder. To exploit time–frequency diversity and combat multipath fading, the coded bits are further interleaved according to some preferred time–frequency patterns, and the resulting bit sequence is mapped into constellation symbols and then converted into a block of N symbols $x[0], x[1], \ldots, x[N-1]$ by the serial-to-parallel converter. The N symbols are the frequency components to be transmitted using the N subcarriers of the OFDM modulator and are converted to OFDM symbols $X[0], X[1], \ldots, X[N-1]$ by the unitary inverse fast Fourier transform (IFFT), i.e.,

$$X[n] = \frac{1}{\sqrt{N}} \sum_{k=0}^{N-1} x[k] e^{j\frac{2\pi nk}{N}}, \qquad n = 0, 1, \ldots, N-1.$$

A cyclic prefix of length P $(P \leq N)$ is added to the IFFT output to eliminate the intersymbol interference caused by multipath propagation. The resulting $N+P$ symbols are converted into a continuous-time baseband signal $x(t)$ for transmission. At the demodulator, after removing the cyclic prefix, the unitary fast Fourier transform is performed on the remaining N symbols to obtain

$$y[k] = H[k]x[k] + w[k], \qquad k = 0, 1, \ldots, N-1 \quad (1)$$

where $x[k]$ is the transmitted data symbol in the kth subcarrier, $H[k]$ is the channel response in the kth subcarrier, and $w[k]$ is the additive noise component in the kth subcarrier. Note that $H[k]$, $k = 0, 1, \ldots, N-1$, are the Fourier transform coefficients of the discrete-time baseband channel impulse response $h[n]$, i.e.,

$$H[k] = \sum_{n=0}^{P-1} h[n] e^{-j\frac{2\pi kn}{N}}, \qquad k = 0, 1, \ldots, N-1. \tag{2}$$

From (1), $x[k]$ can be simply estimated from

$$\widehat{x}[k] = \frac{y[k]}{H[k]}, \qquad k = 0, 1, \ldots, N-1.$$

The obtained symbols are then mapped into bits, and the resulting bit sequence is deinterleaved and decoded to get back the information bits.

The OFDM scheme converts a frequency-selective channel into a set of separate flat-fading subchannels. In Section III, we analyze its performance in indoor environments and derive the maximum range for which reliable communication can be achieved with limited transmission power.

III. Performance Analysis

To examine the system performance, we need to choose a channel model that allows us to investigate the signal propagation in indoor environments. The IEEE 802.15.3a working group proposed an indoor UWB channel model for the evaluation of different UWB system proposals [11]. Our performance analysis is based on the proposed model.

A. S–V Model

In the model, the impulse response of the multipath channel is modeled as

$$h(t) = X \sum_{l=0}^{L} \sum_{m=0}^{M} \alpha_{m,l} \delta(t - T_l - \tau_{m,l}) \tag{3}$$

where $\alpha_{m,l}$ is the multipath gain coefficient, T_l is the arrival time of the lth cluster, $\tau_{m,l}$ is the arrival time (in relation to T_l) of the mth multipath component in the lth cluster, and X represents the lognormal shadowing. The distribution of the cluster arrival time and the ray arrival time is

$$\begin{aligned} p(T_l | T_{l-1}) &= \Lambda e^{-\Lambda(T_l - T_{l-1})} \\ p(\tau_{m,l} | \tau_{m-1,l}) &= \lambda e^{-\lambda(\tau_{m,l} - \tau_{m-1,l})} \end{aligned} \tag{4}$$

where Λ and λ are the cluster arrival rate and the ray arrival rate, respectively, and $T_0 = 0$ and $\tau_{0,l} = 0$. The multipath gain coefficient is modeled as

$$\alpha_{m,l} = p_{m,l} \xi_l \beta_{m,l}$$

where $p_{m,l}$ is equiprobably ± 1 to model signal inversion caused by reflections, ξ_l models the fading related to the lth cluster, and $\beta_{m,l}$ models the fading related to the mth ray of the lth cluster. The small-scale fading coefficient $\xi_l \beta_{m,l}$ is modeled as a lognormal random variable, i.e.,

$$20 \log_{10}(\xi_l \beta_{m,l}) \sim \mathcal{N}\left(\mu_{m,l}, \sigma_1^2 + \sigma_2^2\right) \tag{5}$$

where σ_1^2 and σ_2^2 account for the fading contributed by the cluster and the ray, respectively. Moreover, the profile of the power decay along different propagation paths is modeled as

$$\mathbf{E}\left\{\alpha_{m,l}^2\right\} = \mathbf{E}\left\{\xi_l^2 \beta_{m,l}^2\right\} = \Omega_0 e^{-\frac{T_l}{\Gamma}} e^{-\frac{\tau_{m,l}}{\gamma}} \tag{6}$$

where Γ and γ are constants that characterize the exponential decay of each cluster and each ray in its associated cluster, and Ω_0 is a constant. From (5) and (6), we have

$$\mu_{m,l} = \frac{10 \ln(\Omega_0) - \frac{10T_l}{\Gamma} - \frac{10\tau_{m,l}}{\gamma}}{\ln(10)} - \frac{\left(\sigma_1^2 + \sigma_2^2\right)\ln(10)}{20}.$$

For each realization, the total energy contained in the terms $\alpha_{m,l}$ is normalized to unity, i.e.,

$$\sum_{l=0}^{L} \sum_{m=0}^{M} \alpha_{m,l}^2 = 1. \tag{7}$$

This is because the actual energy of multipath propagation will be accounted for by the link budget that will be explained in Section III-C4. The large-scale fading coefficient X is also modeled as a lognormal random variable, i.e.,

$$20 \log_{10} X \sim \mathcal{N}\left(0, \sigma_x^2\right).$$

The constant parameters in this model can be specified to account for different indoor environments. The IEEE 802.15.3a working group defined four types of indoor channels, namely CM1, CM2, CM3, and CM4 models [11]. CM1 describes a line-of-sight (LOS) scenario when the distance between the transmitter and the receiver is less than 4 m, whereas CM2 describes a non-LOS scenario for the same range. CM3 models a non-LOS situation when the range is between 4 and 10 m, and CM4 models an environment with strong delay dispersion. The model parameters for the four types of S–V channels are listed in Table I.

B. Statistical Characteristics of $H[k]$

Given the S–V model (3), we can characterize the distribution of the Fourier transform coefficients $H[k]$, $k = 0, 1, \ldots, N-1$, of the discrete-time baseband channel impulse response $h[n]$. It can be derived from (2) for $H[k]$ that (see Appendix A for derivation)

$$\mathbf{E}\{H[k]\} = 0 \quad \text{and} \quad \mathbf{E}\left\{|H[k]|^2\right\} = e^{0.0265\sigma_x^2}. \tag{8}$$

When L and M are large, it is reasonable to assume that $H[k]$ is circularly symmetric and Gaussian distributed by the central limit theorem. Hence, $|H[k]|$ is approximately Rayleigh distributed, and the probability density function of $|H[k]|^2$ can be approximated by the exponential distribution

$$p\left(|H[k]|^2\right) \approx \frac{1}{\mathbf{E}\left\{|H[k]|^2\right\}} e^{-\frac{|H[k]|^2}{\mathbf{E}\{|H[k]|^2\}}} \tag{9}$$

TABLE I
TABLE OF CHANNEL MODEL PARAMETERS

	CM1	CM2	CM3	CM4
Λ (ns^{-1})	0.0233	0.4	0.067	0.067
λ (ns^{-1})	2.5	0.5	2.1	2.1
Γ	7.1	5.5	14.0	24.0
γ	4.3	6.7	7.9	12.0
σ_1	3.4	3.4	3.4	3.4
σ_2	3.4	3.4	3.4	3.4
σ_x	3	3	3	3
Ω_0	1	1	1	1
$\mathbf{E}\{H[k]\}$	0	0	0	0
$\mathbf{E}\{\mid H[k]\mid^2\}$	1.269	1.269	1.269	1.269
$\mid \mathrm{cor}\{H[k_1], H[k_2]\}\mid \leq 0.5$	$\mid\overline{k}_1 - \overline{k}_2\mid \geq 13$	$\mid\overline{k}_1 - \overline{k}_2\mid \geq 7$	$\mid\overline{k}_1 - \overline{k}_2\mid \geq 5$	$\mid\overline{k}_1 - \overline{k}_2\mid \geq 3$
Coherence Bandwidth (MHz)	53.6	28.9	20.6	12.4

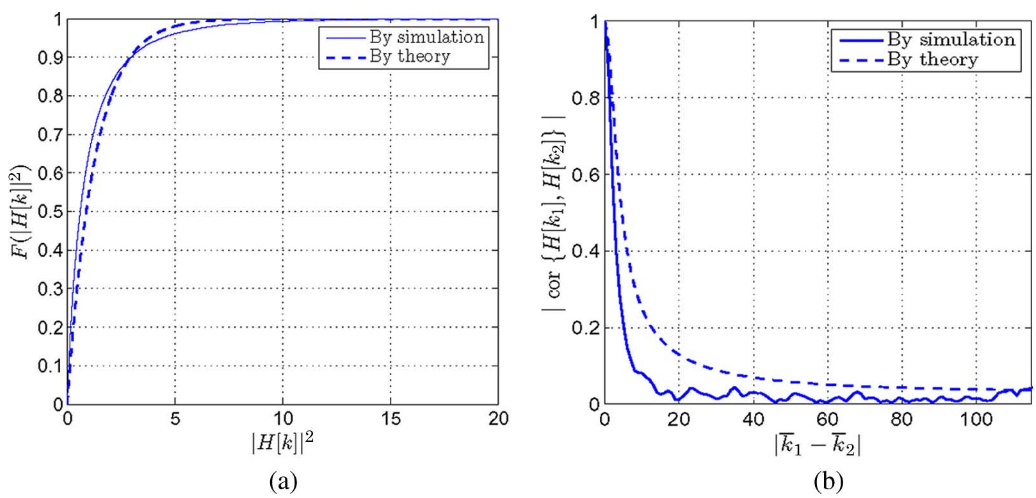

Fig. 2. Statistical characteristics of the impulse response of the CM3-type channels in the frequency domain. (a) Distribution of $|H[k]|^2$. (b) Cross-correlation of $H[k]$.

or, equivalently, the cumulative distribution function of $|H[k]|^2$ is approximated by

$$F\left(|H[k]|^2\right) \approx 1 - e^{-\frac{|H[k]|^2}{\mathbf{E}\{|H[k]|^2\}}} \tag{10}$$

where $\mathbf{E}\{|H[k]|^2\}$ is given by (8). This approximation plays an important role in our analysis. To illustrate this approximation, Fig. 2(a) shows the cumulative distribution function of $|H[k]|^2$ over 500 realizations for the four types of S–V channels. It can be seen that the approximation made in (10) is close to the true distribution.

Another useful statistical measure is the normalized cross correlation of $H[k]$, and its amplitude is approximated by (see Appendix B for derivation)

$$\begin{aligned}
&|\mathrm{cor}\{H[k_1], H[k_2]\}| \\
&= \left| \frac{\mathbf{E}\{H[k_1]H^*[k_2]\}}{\mathbf{E}\left\{|H[k]|^2\right\}} \right| \\
&\approx \left| \frac{1 + \frac{\Lambda\Gamma}{1 + j\frac{2\pi(\overline{k}_1 - \overline{k}_2)\Gamma}{NT_s}}}{1 + \Lambda\Gamma} \right| \left| \frac{1 + \frac{\lambda\gamma}{1 + j\frac{2\pi(\overline{k}_1 - \overline{k}_2)\gamma}{NT_s}}}{1 + \lambda\gamma} \right|
\end{aligned} \tag{11}$$

where $\overline{k}_i$ is related to k_i by

$$\overline{k}_i = \begin{cases} k_i, & 0 \leq k_i \leq \frac{N}{2} - 1 \\ k_i - N, & \frac{N}{2} \leq k_i \leq N - 1 \end{cases}$$

for $i = 1, 2$. In Fig. 2(b), $|\mathrm{cor}\{H[k_1], H[k_2]\}|$ is plotted for the CM3-type channels with $T_s = 1/528$ μs and $N = 128$. Two subcarriers k_1 and k_2 will be regarded as uncorrelated if their normalized cross correlation is small in amplitude. It is conventionally assumed that two subcarriers k_1 and k_2 are uncorrelated if $|\mathrm{cor}\{H[k_1], H[k_2]\}| \leq 0.5$. Thus, we can compute the coherence bandwidth for the four types of S–V channels using (11), and the numerical results for $T_s = 1/528$ μs and $N = 128$ are summarized in Table I. For the CM3-type channels, two subcarriers are uncorrelated if $|\overline{k}_1 - \overline{k}_2| \geq 5$. Given that $T_s = 1/528$ μs, the coherence bandwidth is approximately equal to $(5/128) \times 528 = 20.6$ MHz.

Remark: It is seen in Table I that the four types of S–V channels have the same $\mathbf{E}\{|H[k]|^2\}$ and, hence, have the same distribution on $|H[k]|^2$, as given in (9) and (10). The difference among the four types of S–V channels lies in the normalized cross correlation between different subcarriers, which determines the coherence bandwidth of a wireless channel.

C. Average BER and PER

Using the distribution of $|H[k]|^2$, we can now evaluate the average BER and PER of the MB-OFDM UWB scheme. In the following analysis, we assume a quaternary phase-shift keying (QPSK) constellation, which has been adopted by the IEEE 802.15.3a working group. We also assume that the receiver has perfect channel information.

1) Average Uncoded BER: The uncoded BER is defined as the BER before the convolutional decoder. Using (9), we are able to calculate the average uncoded BER as (see [12, pp. 52–56] for derivation)

$$\begin{aligned}\mathrm{BER}_{\mathrm{uc}} &= \mathbf{E}\left\{Q\left(\sqrt{2|h|^2\mathrm{SNR}_r}\right)\right\}\\ &= \frac{1}{2}\left(1-\sqrt{\frac{\mathrm{SNR}_r}{1+\mathrm{SNR}_r}}\right)\end{aligned} \tag{12}$$

where $Q(\cdot)$ is the complementary cumulative distribution function of the standard normal distribution, $\mathrm{SNR}_r = E_b/N_0$ is the SNR at the receiver, E_b is the average received energy per bit, and N_0 is the single-sided power spectral density of the additive white Gaussian noise, i.e., the noise variance. Here, h is circularly Gaussian distributed with $\mathbf{E}\{|h|^2\} = 1$.

2) Average Coded BER: The coded BER is defined as the BER after the convolutional decoder. In the MB-OFDM UWB proposal, a rate-1/3 convolutional encoder with

$$\begin{aligned}G(D) = [&1 + D^2 + D^3 + D^5 + D^6\\ &1 + D + D^2 + D^4 + D^6\\ &1 + D + D^2 + D^3 + D^6]\end{aligned} \tag{13}$$

is used for the data rate of 110 Mb/s. It is found for this particular $G(D)$ that

$$d_{\mathrm{free}} = 15 \quad \text{and} \quad N_b = 7$$

where d_{free} is the minimum free distance of the convolutional code, and N_b is the sum of the Hamming weight of all the input sequences whose associated convolutional codewords have a Hamming weight of d_{free}. Assume that the convolutional encoder is followed by an *ideal* time–frequency interleaver. Then, each coded bit has an equal probability of being wrongly decoded, and the average coded BER is bounded by

$$\mathrm{BER}_c \le \left.\frac{\partial T(W,I)}{\partial I}\right|_{I=1,\, W=\sqrt{4\mathrm{BER}_{\mathrm{uc}}(1-\mathrm{BER}_{\mathrm{uc}})}} \tag{14}$$

where $T(W,I)$ is the generating function of the convolutional encoder [13]. Expression (14) can be approximated by

$$\mathrm{BER}_c \approx N_b\left[4\mathrm{BER}_{\mathrm{uc}}(1-\mathrm{BER}_{\mathrm{uc}})\right]^{\frac{d_{\mathrm{free}}}{2}} \tag{15}$$

and, therefore, we arrive at

$$\mathrm{BER}_c \approx N_b(1+\mathrm{SNR}_r)^{-\frac{d_{\mathrm{free}}}{2}}.$$

3) Average PER: Assume that each packet consists of U information bits, and each information bit has the same probability of being wrongly decoded. This is a reasonable assumption because of the use of the bit scrambler and interleaver. Hence, the average PER can be computed as

$$\mathrm{PER} = 1 - (1 - \mathrm{BER}_c)^U \tag{16}$$

which gives

$$\mathrm{PER} \approx 1 - \left[1 - N_b(1+\mathrm{SNR}_r)^{-\frac{d_{\mathrm{free}}}{2}}\right]^U.$$

In the MB-OFDM UWB proposal, each packet has 1024 bytes of data, and therefore, $U = 8192$.

4) Link Budget: The aforementioned analysis shows how the BER and the PER relate to $\mathrm{SNR}_r = E_b/N_0$. We now examine their dependence on the range of transmission d. Since the S–V channel model does not take into account the issue of link budget, e.g., the path loss and the noise figure, we have to consider the transmission and reception of radio signals in real situations [7].

To begin with, since the transmission power cannot exceed the specified -41.25 dBm/MHz, the average transmitted power should satisfy

$$P_{\mathrm{TX}} \le -41.25 + 10\,\log_{10}(f_U - f_L)\ (\mathrm{dBm}) \tag{17}$$

where f_U and f_L are the upper and lower frequencies in terms of megahertz of the transmission spectrum, respectively. Moreover, the signal attenuation during transmission is modeled by the path loss

$$P_L = 20\,\log_{10}\left(\frac{4\pi f_g d}{c}\right) \quad \text{(in decibels)}$$

where c is the speed of light, and f_g is the geometric average of f_U and f_L, i.e., $f_g = \sqrt{f_U f_L}$. At the receiver, the average noise power per bit can be computed using the formula $-174 + 10\,\log_{10} R_b$ (in dBm). Here, R_b is the data rate in bits per second, and -174 comes from $k_B T$ calculated at room temperature as the thermal noise power per hertz, where $k_B = 1.38 \times 10^{-23}$ J/K is the Boltzmann's constant, and T is the temperature in kelvins. Therefore, if we assume that the noise figure of the antenna and the receiver RF chain is 6.6 dB, and the implementation loss in the digital baseband is 2.5 dB [7], then we have

$$\begin{aligned}\mathrm{SNR}_r &= \frac{E_b}{N_0}\\ &= P_{\mathrm{TX}} - 20\,\log_{10}\left(\frac{4\pi f_g d}{c}\right) - (-174 + 10\,\log_{10}(R_b))\\ &\quad - 6.6 - 2.5 + 10\,\log_{10}\left(\mathbf{E}\left\{|H[k]|^2\right\}\right) \quad \text{(in decibels)}\end{aligned} \tag{18}$$

where the term $10\,\log_{10}(\mathbf{E}\{|H[k]|^2\})$ is the fading gain that is captured by the S–V channel model.

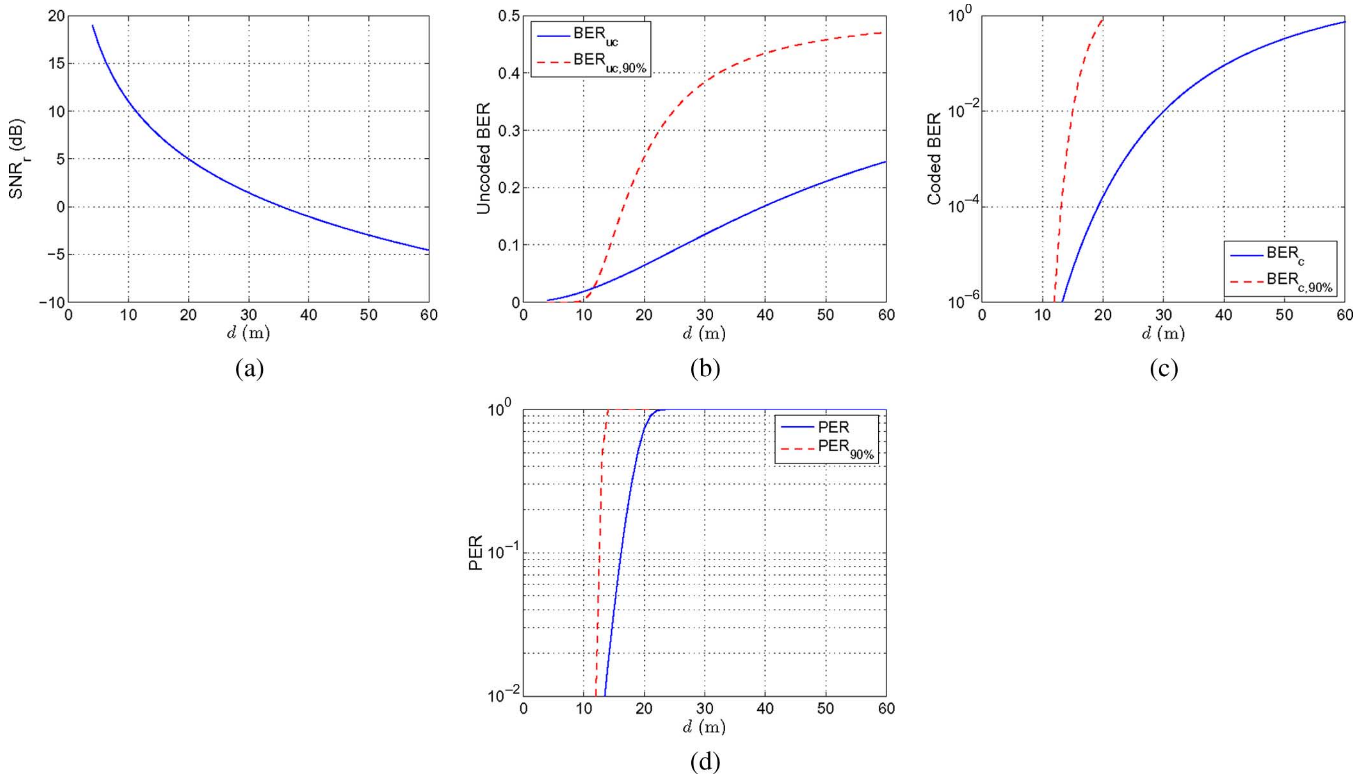

Fig. 3. Plots of SNR_r and the theoretical BERs and PERs versus the transmission distance d when $P_{\mathrm{TX}} = -10.3$ dBm, $R_b = 110$ Mb/s, $f_L = 3.1$ GHz, and $f_U = 4.8$ GHz for the CM1–CM4 channels. (a) Received SNR. (b) Uncoded BER. (c) Coded BER. (d) PER.

As a consequence of the aforementioned derivation, the average PER is related to the transmission distance d by

$$\mathrm{PER} \approx 1 - \left[1 - N_b(1+\mathrm{SNR}_r)^{-\frac{d_{\mathrm{free}}}{2}}\right]^U \tag{19}$$

where SNR_r is given by (18).

D. Ninetieth-Percentile BER and PER

In addition to the average BER and PER performance, we are also interested in another form of performance measure that gives an indication of the probability of channel failure. For this purpose, the so-called "ninetieth-percentile BER (or PER) performance" [7] is defined as the BER (or PER) level such that the MB-OFDM scheme will perform better than for at least 90% of the channel realizations. Since it is cumbersome to explicitly compute the ninetieth-percentile performance measure, we shall approximate it as follows: We first identify the cutoff channel gain such that 90% of the subcarrier channel realizations will exceed it. This is found from (10) by setting

$$F\left(|H_{90\%}[k]|^2\right) \approx 1 - e^{-\frac{|H_{90\%}[k]|^2}{\mathbf{E}\{|H[k]|^2\}}} = 0.10$$

i.e., the cutoff gain is

$$|H_{90\%}[k]|^2 = -\ln(0.9)\,\mathbf{E}\left\{|H[k]|^2\right\} = 0.105\,\mathbf{E}\left\{|H[k]|^2\right\}.$$

Then, we use this gain to approximate the ninetieth-percentile uncoded BER as

$$\mathrm{BER}_{\mathrm{uc},90\%} \approx Q\left(\sqrt{0.210\,\mathrm{SNR}_r}\right)$$

and the associated ninetieth-percentile PER as

$$\mathrm{PER}_{90\%} \approx 1 - \left[1 - N_b\left[4\,\mathrm{BER}_{\mathrm{uc},90\%}(1-\mathrm{BER}_{\mathrm{uc},90\%})\right]^{\frac{d_{\mathrm{free}}}{2}}\right]^U. \tag{20}$$

In Fig. 3, the theoretical BERs and PERs are plotted as functions of d when $P_{\mathrm{TX}} = -10.3$ dBm, $R_b = 110$ Mb/s, $f_L = 3.1$ GHz, and $f_U = 4.8$ GHz for the CM1–CM4 channels. Since the four types of S–V channels have approximately an identical distribution on $|H[k]|^2$, the MB-OFDM scheme performs similarly well for each of them.

IV. Range Improvement

It is seen from (19) that the use of a convolutional code with a bit interleaver for OFDM modulation can achieve a coding gain that is represented by the exponent of the SNR_r term, i.e., $d_{\mathrm{free}}/2$. However, in UWB systems, there exists rich spectral and spatial diversity that may exceed what can be achieved by a convolutional code of moderate complexity. For example, the coherence bandwidth of the CM3-type channels is about 20.6 MHz, which is much smaller than the bandwidth of each subband, i.e., 528 MHz. Moreover, from (15), we notice that a small improvement in the uncoded BER will benefit the overall system performance, such as the PER, significantly through the exponential effect. This observation motivates us to improve the uncoded BER by exploiting the spectral and spatial diversity. In this section, we illustrate how to use linear precoding [9] and multiple antennas [10] to improve the transmission range. One important advantage of the methods is that they can be directly applied to the MB-OFDM scheme. Although the approaches we are pursuing here are well known in the literature, the theoretical and simulated results provide useful insights for the case of real UWB systems.

A. Linear Precoding Over Parallel Subcarriers

It can be seen from (1) that in the original MB-OFDM scheme, each QPSK symbol $x[k]$ is transmitted using only one subcarrier, so that the uncoded BER given by (12) is relatively high due to the occurrence of deep fades, i.e., when $|H[k]|$ is small. We can improve the uncoded BER by spreading each QPSK symbol to several uncorrelated subcarriers. Such "symbol spreading" can be achieved by linear precoding, as was suggested in [9] in another context.

Assume that we intend to send S symbols using J independent subcarriers ($J \geq S$). Instead of transmitting the original constellation symbols, we send rotated symbols that are obtained by

$$\begin{aligned}&[\,x'[k_1] \quad x'[k_2] \quad \cdots \quad x'[k_J]\,]^T\\ &\qquad = \mathbf{A} \times [\,x[k_1] \quad x[k_2] \quad \cdots \quad x[k_s]\,]^T\end{aligned}$$

where $\mathbf{A}^*\mathbf{A} = (J/S) \times \mathbf{I}_S$, and $\mathbf{A}$ is selected to maximize the minimum product distance between any two rotated code vectors, i.e.,

$$\begin{aligned}\mathbf{A}_{\rm opt} &= \arg\max_{\mathbf{A}} \min_{\mathbf{x}'_1 \neq \mathbf{x}'_2} \prod_{j=1}^{J} |x'_1[k_J] - x'_2[k_J]|\\ \text{subject to} \quad & \mathbf{A}^*\mathbf{A} = \frac{J}{S} \times \mathbf{I}_S \qquad (21)\end{aligned}$$

where $\mathbf{x}'_i = [\,x'_i[k_1] \quad x'_i[k_2] \quad \cdots \quad x'_i[k_J]\,]^T$, $i = 1, 2$, are two rotated code vectors. The problem formulated by (21) is a nonconvex multidimensional optimization problem, and the optimal $\mathbf{A}_{\rm opt}$ is usually found by exhaustive search. The original symbols can be optimally decoded by maximum-likelihood decoding, but the complexity will grow exponentially with the size of $\mathbf{A}$. Sphere decoding can be used as a suboptimal approximation to the maximum-likelihood decoding at a relatively lower complexity [14], [15].

1) Case 1 ($S = 2$ and $J = 2$): As discussed in Section III-B, two subcarriers can be treated as independent if the difference in their subcarrier frequencies is greater than the coherence bandwidth of the channel. To implement the precoding scheme with $S = 2$ and $J = 2$, we group the subcarriers in a subband according to the pairing $(k, k + (N/2))$, $k = 0, 1, \ldots, (N/2) - 1$. The symbols $x[k]$ and $x[k + (N/2)]$ are converted to $x'[k]$ and $x'[k + (N/2)]$ by

$$\begin{bmatrix} x'[k] \\ x'\left[k + \frac{N}{2}\right] \end{bmatrix} = \mathbf{A} \begin{bmatrix} x[k] \\ x\left[k + \frac{N}{2}\right] \end{bmatrix}$$

and $x'[k]$ and $x'[k + (N/2)]$ are transmitted over subcarriers k and $k + (N/2)$, respectively. Note that $\mathbf{A}$ is unitary, and hence, the total transmission power is preserved after the transformation. By solving (21), an optimal rotation matrix $\mathbf{A}_{\rm opt}$ is given by

$$\mathbf{A}_{\rm opt} = \begin{bmatrix} 0.707 & 0.5 - 0.5j \\ -0.5 - 0.5j & 0.707 \end{bmatrix}.$$

2) Case 2 ($S = 3$ and $J = 3$): In this case, we group the subcarriers in a subband according to the pairing $(k, k + \lfloor N/3 \rfloor, k + 2\lfloor N/3 \rfloor)$, $k = 0, 1, \ldots, \lfloor N/3 \rfloor - 1$. Then, $x[k]$, $x[k + \lfloor N/3 \rfloor]$, and $x[k + 2\lfloor N/3 \rfloor]$ are converted to $x'[k]$, $x'[k + \lfloor N/3 \rfloor]$, and $x'[k + 2\lfloor N/3 \rfloor]$, respectively, by

$$\begin{bmatrix} x'[k] \\ x'\left[k + \left\lfloor \frac{N}{3} \right\rfloor\right] \\ x'\left[k + 2\left\lfloor \frac{N}{3} \right\rfloor\right] \end{bmatrix} = \mathbf{A} \begin{bmatrix} x[k] \\ x\left[k + \left\lfloor \frac{N}{3} \right\rfloor\right] \\ x\left[k + 2\left\lfloor \frac{N}{3} \right\rfloor\right] \end{bmatrix}$$

and $x'[k]$, $x'[k + \lfloor N/3 \rfloor]$, and $x'[k + 2\lfloor N/3 \rfloor]$ are transmitted over subcarriers k, $k + \lfloor N/3 \rfloor$, and $k + 2\lfloor N/3 \rfloor$, respectively. The optimal rotation matrix $\mathbf{A}_{\rm opt}$ is

$$\begin{aligned}&\mathbf{A}_{\rm opt}\\ &= \begin{bmatrix} 0.687 & 0.513 - 0.113j & -0.428 + 0.264j \\ -0.358 - 0.308j & 0.696 - 0.172j & -0.011 - 0.513j \\ 0.190 + 0.520j & 0.243 - 0.389j & 0.696 \end{bmatrix}.\end{aligned}$$

3) Performance Analysis: Since it is difficult to obtain a simple closed-form expression for the uncoded BER when linear precoding is used, we characterize its performance by considering the union bound of symbol detection errors. Let $\mathbf{x}_i = [\,x_i[k_1] \quad x_i[k_2] \quad \cdots \quad x_i[k_S]\,]^T$, $i = 1, 2$, be any two different code vectors, and let $\mathbf{x}'_i = [\,x'_i[k_1] \quad x'_i[k_2] \quad \cdots \quad x'_i[k_J]\,]^T$, $i = 1, 2$, be the corresponding rotated code vectors. Without loss of generality, we assume that the energy of each element of $\mathbf{x}_i$ is normalized, i.e., $|x_i[k_s]|^2 = 1$, $s = 1, 2, \ldots, S$. Then, the pairwise error probability between $\mathbf{x}'_1$ and $\mathbf{x}'_2$ is given by

$$\begin{aligned}P_e &= \mathbf{E}\left\{ Q\left(\sqrt{\sum_{j=1}^{J} |\,h[k_j]|^2\, |x'_1[k_j] - x'_2[k_j]|^2\, \mathrm{SNR}_r} \right) \right\}\\ &< 2^J \left(\prod_{j=1}^{J} |x'_1[k_j] - x'_2[k_j]| \right)^{-2} \mathrm{SNR}_r^{-J} \qquad (22)\end{aligned}$$

where $h[k_j]$ are circularly Gaussian distributed with $\mathbf{E}\{|h[k_j]|^2\} = 1$ for $j = 1, 2, \ldots, J$. From this expression, we can see that maximizing the minimum product distance is equivalent to minimizing the maximum bound given by (22) on the pairwise error probability between any two code vectors. Usually, the average BER is dominated by the error events that have the maximum pairwise error probability, and hence, the

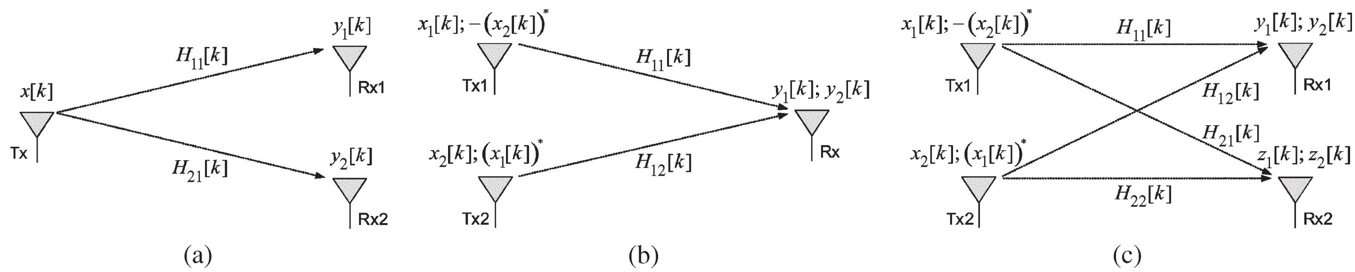

Fig. 4. MIMO schemes. (a) 1Tx2Rx configuration. (b) 2Tx1Rx configuration. (c) 2Tx2Rx configuration.

use of linear precoding is able to improve the overall system performance.

B. MIMO Scheme

We now examine how to employ multiple transmit and receive antennas to improve the UWB transmission range.

1) One Transmit and Two Receive Antennas (1Tx2Rx): In the configuration shown in Fig. 4(a), two antennas are used to receive the signals from the transmit antenna, which can be formulated as

$$\begin{bmatrix} y_1[k] \\ y_2[k] \end{bmatrix} = \begin{bmatrix} H_{11}[k] \\ H_{21}[k] \end{bmatrix} x[k] + \begin{bmatrix} w_1[k] \\ w_2[k] \end{bmatrix}$$

for $k = 0, 1, \ldots, N-1$. At the receiver, the transmitted symbol $x[k]$ can be estimated from the output of the maximal ratio combiner [16]

$$\widehat{x}[k] = H_{11}^*[k]y_1[k] + H_{21}^*[k]y_2[k]. \tag{23}$$

2) Two Transmit and One Receive Antennas (2Tx1Rx): In the configuration shown in Fig. 4(b), the Alamouti transmit–diversity scheme is exploited [17]. At block time i, the symbols $x_1[k]$ and $x_2[k]$ are transmitted by the first and second transmit antennas, respectively; at block time $i+1$, the symbols $-(x_2[k])^*$ and $(x_1[k])^*$ are transmitted by the first and second transmit antennas, respectively. Consequently, the received data from two consecutive blocks are

$$\begin{bmatrix} y_1[k] \\ (y_2[k])^* \end{bmatrix} = \begin{bmatrix} H_{11}[k] & H_{12}[k] \\ H_{12}^*[k] & -H_{11}^*[k] \end{bmatrix} \begin{bmatrix} x_1[k] \\ x_2[k] \end{bmatrix} + \begin{bmatrix} w_1[k] \\ (w_2[k])^* \end{bmatrix}$$

At the receiver, $x_1[k]$ and $x_2[k]$ are decoded from

$$\begin{aligned} \widehat{x}_1[k] &= H_{11}^*[k]y_1[k] + H_{12}[k]\left(y_2[k]\right)^* \\ \widehat{x}_2[k] &= H_{12}^*[k]y_1[k] - H_{11}[k]\left(y_2[k]\right)^*. \end{aligned}$$

3) Two Transmit and Two Receive Antennas (2Tx2Rx): With two transmit and two receive antennas, as shown in Fig. 4(c), we again exploit the Alamouti transmission scheme to get

$$\begin{aligned} \begin{bmatrix} y_1[k] \\ (y_2[k])^* \end{bmatrix} &= \begin{bmatrix} H_{11}[k] & H_{12}[k] \\ H_{12}^*[k] & -H_{11}^*[k] \end{bmatrix} \begin{bmatrix} x_1[k] \\ x_2[k] \end{bmatrix} + \begin{bmatrix} w_1[k] \\ (w_2[k])^* \end{bmatrix} \\ \begin{bmatrix} z_1[k] \\ (z_2[k])^* \end{bmatrix} &= \begin{bmatrix} H_{21}[k] & H_{22}[k] \\ H_{22}^*[k] & -H_{21}^*[k] \end{bmatrix} \begin{bmatrix} x_1[k] \\ x_2[k] \end{bmatrix} + \begin{bmatrix} v_1[k] \\ (v_2[k])^* \end{bmatrix}. \end{aligned}$$

At the receiver, $x_1[k]$ and $x_2[k]$ are decoded from

$$\begin{aligned} \widehat{x}_1[k] &= H_{11}^*[k]y_1[k] + H_{12}[k]\left(y_2[k]\right)^* + H_{21}^*[k]z_1[k] \\ &\quad + H_{22}[k]\left(z_2[k]\right)^* \\ \widehat{x}_2[k] &= H_{12}^*[k]y_1[k] - H_{11}[k]\left(y_2[k]\right)^* + H_{22}^*[k]z_1[k] \\ &\quad - H_{21}[k]\left(z_2[k]\right)^*. \end{aligned}$$

4) Performance Analysis: To analyze the performance of the MIMO schemes, we assume that $H_{lj}[k]$ are statistically independent of each other for different (l, j) pairs. It can then be shown that the average uncoded BERs are (see Appendix C for derivation)

$$\begin{aligned} \mathrm{BER}_{\mathrm{uc}}^{\mathrm{1Tx2Rx}} &= \frac{1}{2} - \frac{3}{4}\mu + \frac{1}{4}\mu^3 \\ \mathrm{BER}_{\mathrm{uc}}^{\mathrm{2Tx1Rx}} &= \frac{1}{2} - \frac{3}{4}\mu' + \frac{1}{4}\mu'^3 \\ \mathrm{BER}_{\mathrm{uc}}^{\mathrm{2Tx2Rx}} &= \left(\frac{1-\mu'}{2}\right)^4 \left[1 + 4\left(\frac{1+\mu'}{2}\right) + 10\left(\frac{1+\mu'}{2}\right)^2 \right. \\ &\quad \left. + 20\left(\frac{1+\mu'}{2}\right)^3\right] \end{aligned} \tag{24}$$

where

$$\mu = \sqrt{\frac{\mathrm{SNR}_r}{1 + \mathrm{SNR}_r}} \quad \mu' = \sqrt{\frac{0.5\,\mathrm{SNR}_r}{1 + 0.5\,\mathrm{SNR}_r}}$$

and SNR_r is given by (18). The factor "0.5" in μ' is due to the fact that the transmission power of each of the two transmit antennas is only half of that of the one transmit antenna system. The average coded BER and PER can then be computed using (15) and (16), with the average uncoded BER given by (24).

For the ninetieth-percentile performance, we follow the same argument as before to get (see Appendix D for derivation)

$$\begin{aligned} \mathrm{BER}_{\mathrm{uc},90\%}^{\mathrm{1Tx2Rx}} &\approx Q(1.064\,\mathrm{SNR}_r) \\ \mathrm{BER}_{\mathrm{uc},90\%}^{\mathrm{2Tx1Rx}} &\approx Q(0.532\,\mathrm{SNR}_r) \\ \mathrm{BER}_{\mathrm{uc},90\%}^{\mathrm{2Tx2Rx}} &\approx Q(1.745\,\mathrm{SNR}_r). \end{aligned} \tag{25}$$

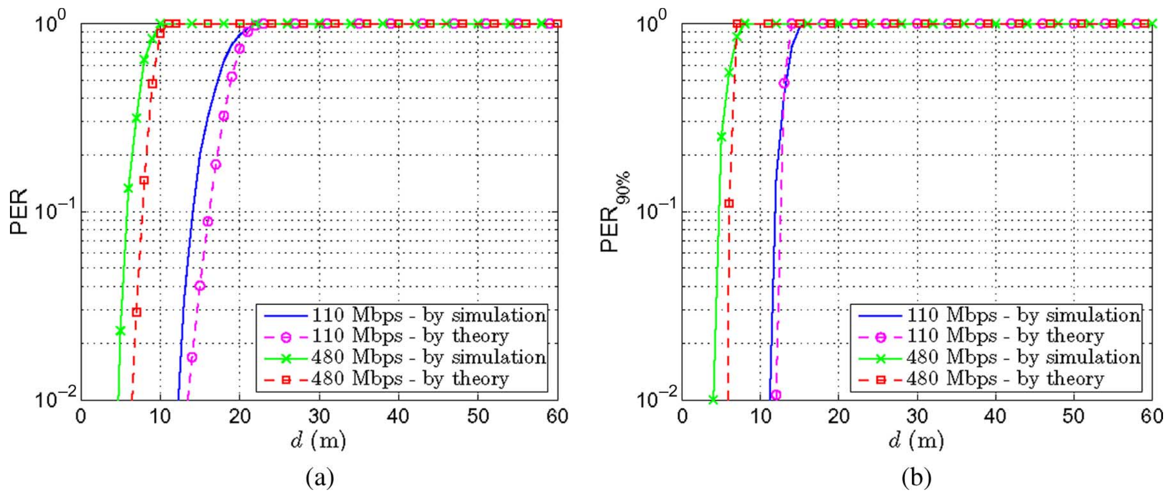

Fig. 5. Average and ninetieth-percentile simulated and theoretical PERs for 110 and 480 Mb/s using one transmit and one receive antennas. (a) Average PER. (b) Ninetieth-percentile PER.

The aforementioned analysis is based on the assumption that $H_{lj}[k]$ are statistically independent; however, in practical situations, $H_{lj}[k]$ might be correlated with each other, and the obtained BER and PER would be larger than expected. Nevertheless, the results obtained here can be viewed as an upper bound on the best performance of the MIMO MB-OFDM system.

V. Computer Simulations

The results derived in the previous sections and the algorithms proposed for range improvement are now verified using computer simulations. The MB-OFDM UWB system proposed by the IEEE 802.15.3a working group is implemented using MATLAB. In the simulations, we utilize the bandwidth from 3.1 to 4.8 GHz with the average transmission power $P_{\mathrm{TX}} = -10.3$ dBm, which satisfies (17). Each data packet consists of 1024 bytes of random bits, so that $U = 8192$. The convolutional encoder is specified by (13), and the standard Viterbi algorithm is used to decode the received bits. A QPSK constellation is used for constellation mapping, and the OFDM symbol size is $N = 128$. For more details about the system, such as the puncturer and the bit interleaver, we refer to [8]. To measure the PER performance, 200 channel realizations are generated according to [11], and for each channel realization, 400 data packets are sent and received using the system. The experimental PERs are computed by comparing the transmitted and received data packets.

In Fig. 5, the average and ninetieth-percentile PERs of the system in the CM3-type channel environment are plotted as functions of the transmission distance for the data rates of 110 and 480 Mb/s. The average and ninetieth-percentile PERs obtained by computer simulations are compared with the theoretical average and ninetieth-percentile PERs that are computed using (19) and (20), respectively. It is seen that (19) and (20) give a good approximation to the true performance of the system. The difference between theory and simulation may come from the assumptions about the distribution of the channel coefficient $H[k]$, the ideal interleaver, and the approximate BER of the convolutional code, etc.

In Fig. 6, the simulated average and ninetieth-percentile PERs in the CM3-type channel environment are plotted versus the transmission distance for the different schemes discussed in this paper and for the data rate of 110 Mb/s. It is seen that the use of linear precoding and multiple antennas can effectively improve the performance of MB-OFDM systems. We also simulated the dual-carrier modulation (DCM) mode that is proposed in the MB-OFDM proposal. It is found that the performance of DCM is slightly better than the QPSK modulation in terms of the average and ninetieth-percentile PERs, whereas the $S = J = 2$ precoding scheme with the optimal rotation matrix $\mathbf{A}_{\mathrm{opt}}$ is obviously better than DCM.[1] Table II lists the maximal transmission range when the required ninetieth-percentile PER is less than 0.08. The use of multiple antennas can improve the reliable transmission range more significantly when compared to linear precoding; however, linear precoding does not require extra antennas and RF links.

Fig. 7 compares the simulated performance of the MIMO schemes with the theoretical performance given by (24) and (25). This comparison indicates that our equations allow us to reasonably well predict the performance of UWB systems.

VI. Conclusion

In this paper, we studied the performance of MB-OFDM UWB systems using the S–V channel model. The derived performance bounds are useful for predicting the behavior of UWB

[1]There is a simple explanation to this observation. For QPSK, DCM, and the $S = J = 2$ linear precoding scheme, the minimum distance between two constellation points (at the receiver side) is the same and equal to $d_{\min} = 2\sqrt{E_b}$. However, the minimum product distance for the three constellation mappings is different: It is zero for QPSK, $1.6E_b$ for DCM, and $2E_b$ for the precoding scheme. For fading channels, the larger the minimum product distance, the better the system performance.

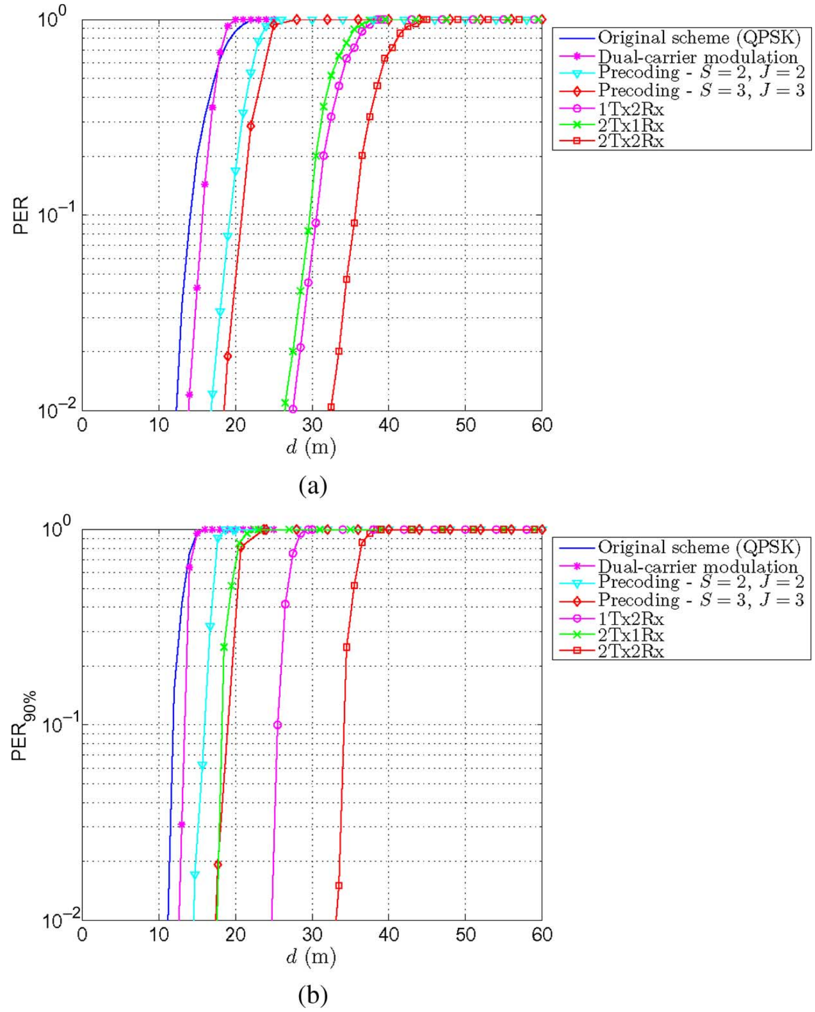

Fig. 6. Average and ninetieth-percentile simulated PERs for $R_b = 110$ Mb/s using linear precoding or multiple antennas. (a) Average PER. (b) Ninetieth-percentile PER.

TABLE II
TABLE OF ACHIEVABLE RANGE FOR A NINETIETH-PERCENTILE PER OF 0.08 WHEN $R_b = 110$ Mb/s

Original scheme (QPSK)	DCM	Precoding - S=2, J=2	Precoding - S=3, J=3	1Tx2Rx	2Tx1Rx	2Tx2Rx
11.8 m	13.3 m	15.8 m	18.8 m	25.4 m	18.1 m	34.0 m

systems in indoor environments, and they have been verified to be consistent with computer simulations. We also analyzed and compared the linear precoding and multiple antenna techniques for transmission range improvement. Linear precoding allows a more efficient use of the rich spectral diversity in UWB systems at the cost of encoding and decoding complexities. The multiple antenna technique exploits the spatial diversity to combat fading and requires extra antennas and RF links. It is shown that both techniques can effectively improve the transmission range of UWB devices.

APPENDIX A
DERIVATION OF (8)

Let $p(t)$ be the baseband pulse shape used in the transmission, T_s be the symbol time, and $h_B(t)$ be the continuous-time impulse response function of the baseband channel. Using (3), the discrete-time baseband channel impulse response $h[n]$ is given by

$$\begin{aligned} h[n] &= \int_{-\infty}^{\infty} h_B(\tau) p(nT_s - \tau) d\tau \\ &= \int_{-\infty}^{\infty} h(\tau) e^{-j2\pi f_c \tau} p(nT_s - \tau) d\tau \\ &= \int_{-\infty}^{\infty} \left(X \sum_{l=0}^{L} \sum_{m=0}^{M} \alpha_{m,l} \delta(\tau - T_l - \tau_{m,l}) \right) e^{-j2\pi f_c \tau} \\ &\quad \times p(nT_s - \tau) d\tau \\ &= \sum_{l=0}^{L} \sum_{m=0}^{M} X \alpha_{m,l} p(nT_s - T_l - \tau_{m,l}) e^{-j2\pi f_c (T_l + \tau_{m,l})}. \end{aligned}$$

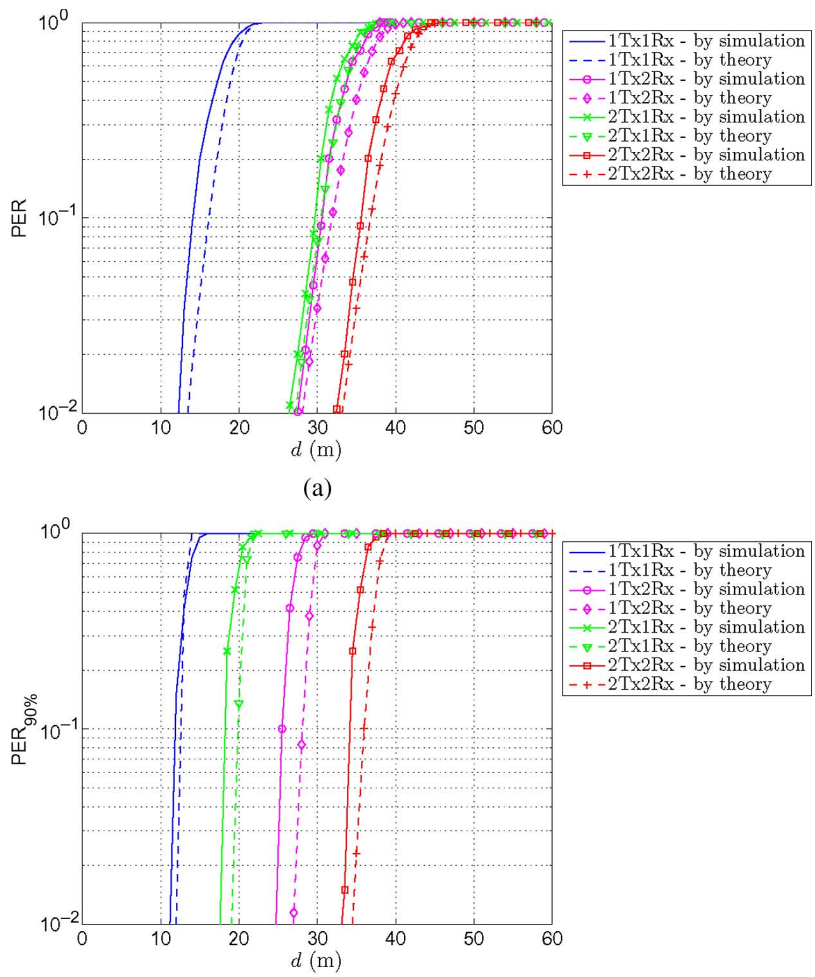

(a)

(b)

Fig. 7. Average and ninetieth-percentile simulated and theoretical PERs for $R_b = 110$ Mb/s using multiple antennas. (a) Average PER. (b) Ninetieth-percentile PER.

The discrete Fourier transform of $h[n]$ is then given by

$$\begin{aligned} H[k] &= \sum_{n=0}^{P-1} h[n] e^{-j\frac{2\pi kn}{N}} \\ &= \sum_{n=-\infty}^{\infty} h[n] e^{-j\frac{2\pi kn}{N}} \\ &= \sum_{n=-\infty}^{\infty} \sum_{l=0}^{L} \sum_{m=0}^{M} X\alpha_{m,l} p(nT_s - T_l - \tau_{m,l}) \\ &\qquad \times e^{-j2\pi\left[\frac{kn}{N} + f_c(T_l + \tau_{m,l}\right]} \end{aligned} \tag{26}$$

because OFDM modulation requires that the length of the cyclic prefix should be longer than that of the channel response, i.e., $h[n] = 0$ if $n \neq 0, 1, \ldots, P-1$. Since $\mathbf{E}\{\alpha_{m,l}\} = 0$, we have $\mathbf{E}\{H[k]\} = 0$. Assume that the baseband pulse shape $p(t)$ used in the transmission scheme has a bandwidth $1/2T_s$ and satisfies the Nyquist criterion, i.e., its Fourier transform $P(f)$ is given by

$$P(f) = \begin{cases} T_s e^{-j2\pi f m_0 T_s}, & -\frac{1}{2T_s} \le f < \frac{1}{2Ts} \\ 0, & \text{otherwise} \end{cases}$$

for some integer m_0. Then, by the sampling theorem

$$\begin{aligned} &\sum_{n=-\infty}^{\infty} p(nT_s - T_l - \tau_{m,l}) e^{-j\frac{2\pi kn}{N}} \\ &\qquad = \begin{cases} e^{-j\frac{2\pi k(m_0 T_s + T_l + \tau_{m,l})}{NT_s}}, & 0 \le k \le \frac{N}{2} - 1 \\ e^{-j\frac{2\pi (k-N)(m_0 T_s + T_l + \tau_{m,l})}{NT_s}}, & \frac{N}{2} \le k \le N-1 \end{cases}. \end{aligned}$$

For convenience of notation, we define $\overline{k}$ as

$$\overline{k} = \begin{cases} k, & 0 \le k \le \frac{N}{2} - 1 \\ k - N, & \frac{N}{2} \le k \le N-1 \end{cases}.$$

Then

$$\sum_{n=-\infty}^{\infty} p(nT_s - T_l - \tau_{m,l}) e^{-j\frac{2\pi kn}{N}} = e^{-j\frac{2\pi \overline{k}(m_0 T_s + T_l + \tau_{m,l})}{NT_s}}. \tag{27}$$

Thus

$$\begin{aligned}
&\mathbf{E}\left\{|H[k]|^2\right\} \\
&= \mathbf{E}\left\{\left|\sum_{n=-\infty}^{\infty}\sum_{l=0}^{L}\sum_{m=0}^{M} X\alpha_{m,l}p(nT_s - T_l - \tau_{m,l}) \times e^{-j2\pi\left[\frac{kn}{N}+f_c(T_l+\tau_{m,l})\right]}\right|^2\right\} \\
&= \mathbf{E}\{X^2\}\mathbf{E}\left\{\left|\sum_{l=0}^{L}\sum_{m=0}^{M}\alpha_{m,l}e^{-j2\pi f_c(T_l+\tau_{m,l})} \times \left(\sum_{n=-\infty}^{\infty} p(nT_s - T_l - \tau_{m,l})e^{-j\frac{2\pi kn}{N}}\right)\right|^2\right\} \\
&= \mathbf{E}\{X^2\}\mathbf{E}\left\{\sum_{l=0}^{L}\sum_{m=0}^{M}|\alpha_{m,l}e^{-j2\pi f_c(T_l+\tau_{m,l})}|^2 \times \left|\sum_{n=-\infty}^{\infty} p(nT_s - T_l - \tau_{m,l})e^{-j\frac{2\pi kn}{N}}\right|^2\right\} \\
&= \mathbf{E}\{X^2\}\mathbf{E}\left\{\sum_{l=0}^{L}\sum_{m=0}^{M}\left|\alpha_{m,l}e^{-j2\pi f_c(T_l+\tau_{m,l})}\right|^2 \times \left|e^{-j\frac{2\pi\overline{k}(m_0T_s+T_l+\tau_{m,l})}{NT_s}}\right|^2\right\} \\
&= \mathbf{E}\{X^2\} \times \mathbf{E}\left\{\sum_{l=0}^{L}\sum_{m=0}^{M}\alpha_{m,l}^2\right\} \\
&= \mathbf{E}\{X^2\} \\
&= \int_{-\infty}^{\infty}(10^{\frac{x}{20}})^2 \times \frac{1}{\sqrt{2\pi\sigma_x^2}}e^{-\frac{x^2}{2\sigma_x^2}}\,dx \\
&\qquad \left(\text{Here, } x \sim \mathcal{N}\left(0,\ \sigma_x^2\right).\right) \\
&= \frac{1}{\sqrt{2\pi\sigma_x^2}}\int_{-\infty}^{\infty} e^{-\frac{1}{2\sigma_x^2}\left(x-\frac{\sigma_x^2\ln 10}{10}\right)^2+\frac{\sigma_x^2\ln^2 10}{200}}\,dx \\
&= e^{\frac{\sigma_x^2\ln^2 10}{200}} = e^{0.0265\sigma_x^2}
\end{aligned}$$

where $\mathbf{E}\{\sum_{l=0}^{L}\sum_{m=0}^{M}\alpha_{m,l}^2\} = 1$ is due to (7).

APPENDIX B
DERIVATION OF (11)

For each realization of the S–V channel model, the total energy contained in $\alpha_{m,l}$ is normalized to unity, as given in (7). However, this complicates the calculation of $\mathrm{cor}\{H[k_1], H[k_2]\}$, i.e., the ratio between $\mathbf{E}\{H[k_1]H^*[k_2]\}$ and $\mathbf{E}\{|H[k]|^2\}$. To simplify the calculation, we assume that the normalization given by (7) does not significantly affect $\mathrm{cor}\{H[k_1], H[k_2]\}$. This assumption is reasonable because the ratio between $H[k_1]H^*[k_2]$ and $|H[k]|^2$ is not affected by the normalization factor for each individual channel realization. With this assumption, we ignore the normalization in the following derivation. Using (26), we have

$$\begin{aligned}
&\mathbf{E}\left\{H[k_1]H^*[k_2]\right\} \\
&= \mathbf{E}\Bigg\{\left[\sum_{n=-\infty}^{\infty}\sum_{l=0}^{L}\sum_{m=0}^{M} X\alpha_{m,l}p(nT_s - T_l - \tau_{m,l}) \times e^{-j2\pi\left[\frac{k_1n}{N}+f_c(T_l+\tau_{m,l})\right]}\right] \\
&\qquad \times \left[\sum_{n=-\infty}^{\infty}\sum_{l=0}^{L}\sum_{m=0}^{M} X\alpha_{m,l}p(nT_s - T_l - \tau_{m,l}) \times e^{-j2\pi\left[\frac{k_2n}{N}+f_c(T_l+\tau_{m,l})\right]}\right]^*\Bigg\} \\
&= \mathbf{E}\{X^2\} \\
&\quad \times \mathbf{E}\Bigg\{\left[\sum_{l=0}^{L}\sum_{m=0}^{M}\alpha_{m,l}e^{-j2\pi f_c(T_l+\tau_{m,l})} \times \left(\sum_{n=-\infty}^{\infty} p(nT_s - T_l - \tau_{m,l})e^{-j\frac{2\pi k_1 n}{N}}\right)\right] \\
&\qquad \times \left[\sum_{l=0}^{L}\sum_{m=0}^{M}\alpha_{m,l}e^{-j2\pi f_c(T_l+\tau_{m,l})} \times \left(\sum_{n=-\infty}^{\infty} p(nT_s - T_l - \tau_{m,l})e^{-j\frac{2\pi k_2 n}{N}}\right)\right]^*\Bigg\} \\
&= \mathbf{E}\{X^2\} \\
&\quad \times \mathbf{E}\Bigg\{\sum_{l=0}^{L}\sum_{m=0}^{M}\left|\alpha_{m,l}e^{-j2\pi f_c(T_l+\tau_{m,l})}\right|^2 \times \left(\sum_{n=-\infty}^{\infty} p(nT_s - T_l - \tau_{m,l})e^{-j\frac{2\pi k_1 n}{N}}\right) \\
&\qquad \times \left(\sum_{n=-\infty}^{\infty} p(nT_s - T_l - \tau_{m,l})e^{-j\frac{2\pi k_2 n}{N}}\right)^*\Bigg\} \\
&= \mathbf{E}\{X^2\} \\
&\quad \times \mathbf{E}\left\{\sum_{l=0}^{L}\sum_{m=0}^{M}\alpha_{m,l}^2 e^{-j\frac{2\pi(\overline{k}_1-\overline{k}_2)(m_0T_s+T_l+\tau_{m,l})}{NT_s}}\right\} \qquad (28)
\end{aligned}$$

$$\begin{aligned}
&= \mathbf{E}\{X^2\} \times e^{-j\frac{2\pi(\overline{k}_1-\overline{k}_2)m_0}{N}} \\
&\quad \times \left(\sum_{l=0}^{L}\sum_{m=0}^{M}\mathbf{E}\left\{\Omega_0 e^{-\frac{T_l}{\Gamma}}e^{-\frac{\tau_{m,l}}{\gamma}}e^{-j\frac{2\pi(\overline{k}_1-\overline{k}_2)(T_l+\tau_{m,l})}{NT_s}}\right\}\right) \qquad (29)
\end{aligned}$$

where (28) follows from (27), and (29) follows from (6). Letting $k_1 = k_2 = k$, we have

$$\mathbf{E}\left\{|H[k]|^2\right\} = \mathbf{E}\{X^2\} \times \left(\sum_{l=0}^{L}\sum_{m=0}^{M} \mathbf{E}\left\{\Omega_0 e^{-\frac{T_l}{\Gamma}} e^{-\frac{\tau_{m,l}}{\gamma}}\right\}\right) \tag{30}$$

which is different from (8), because we considered the normalization given by (7) in the derivation of (8), but not in the derivation of (30). Hence, we have $\mathrm{cor}\{H[k_1], H[k_2]\}$, shown at the bottom of the page, where

$$a = \frac{1}{\Gamma} + j\frac{2\pi(\overline{k}_1 - \overline{k}_2)}{NT_s} \quad \text{and} \quad b = \frac{1}{\gamma} + j\frac{2\pi(\overline{k}_1 - \overline{k}_2)}{NT_s}.$$

By (4), we have $\mathbf{E}\{e^{-aT_0}\}$ and $\mathbf{E}\{e^{-aT_l}\}$, shown at the bottom of the page. Thus, $\mathbf{E}\{e^{-aT_l}\} = \Lambda^l/(\Lambda + a)^l$, $l = 0, 1, \ldots, L$.

$$\begin{aligned}
\mathrm{cor}\{H[k_1], H[k_2]\} &= \frac{\mathbf{E}\{H[k_1]H^*[k_2]\}}{\mathbf{E}\left\{|H[k]|^2\right\}} \\
&= e^{-j\frac{2\pi(\overline{k}_1-\overline{k}_2)m_0}{N}} \times \frac{\sum_{l=0}^{L}\sum_{m=0}^{M}\mathbf{E}\left\{\Omega_0 e^{-\frac{T_l}{\Gamma}} e^{-\frac{\tau_{m,l}}{\gamma}} e^{-j\frac{2\pi(\overline{k}_1-\overline{k}_2)(T_l+\tau_{m,l})}{NT_s}}\right\}}{\sum_{l=0}^{L}\sum_{m=0}^{M}\mathbf{E}\left\{\Omega_0 e^{-\frac{T_l}{\Gamma}} e^{-\frac{\tau_{m,l}}{\gamma}}\right\}} \\
&= e^{-j\frac{2\pi(\overline{k}_1-\overline{k}_2)m_0}{N}} \times \frac{\left(\sum_{l=0}^{L}\mathbf{E}\left\{e^{-\frac{T_l}{\Gamma}} e^{-j\frac{2\pi(\overline{k}_1-\overline{k}_2)T_l}{NT_s}}\right\}\right)\left(\sum_{m=0}^{M}\mathbf{E}\left\{e^{-\frac{\tau_{m,l}}{\gamma}} e^{-j\frac{2\pi(\overline{k}_1-\overline{k}_2)\tau_{m,l}}{NT_s}}\right\}\right)}{\left(\sum_{l=0}^{L}\mathbf{E}\left\{e^{-\frac{T_l}{\Gamma}}\right\}\right)\left(\sum_{m=0}^{M}\mathbf{E}\left\{e^{-\frac{\tau_{m,l}}{\gamma}}\right\}\right)} \\
&= e^{-j\frac{2\pi(\overline{k}_1-\overline{k}_2)m_0}{N}} \times \frac{\left(\sum_{l=0}^{L}\mathbf{E}\{e^{-aT_l}\}\right)\left(\sum_{m=0}^{M}\mathbf{E}\{e^{-b\tau_{m,l}}\}\right)}{\left(\sum_{l=0}^{L}\mathbf{E}\left\{e^{-\frac{T_l}{\Gamma}}\right\}\right)\left(\sum_{m=0}^{M}\mathbf{E}\left\{e^{-\frac{\tau_{m,l}}{\gamma}}\right\}\right)}
\end{aligned}$$

$$\begin{aligned}
\mathbf{E}\{e^{-aT_0}\} &= 1 \\
\mathbf{E}\{e^{-aT_l}\} &= \int_0^\infty e^{-aT_l} p(T_l)\, dT_l \\
&= \int_0^\infty\int_0^\infty\int_0^\infty \cdots \int_0^\infty e^{-aT_l} p(T_1, T_2, \ldots, T_l)\, dT_{l-1}\ldots dT_2 dT_1 dT_l \\
&= \int_0^\infty\int_0^{T_l}\int_{T_1}^{T_l} \cdots \int_{T_{l-2}}^{T_l} e^{-aT_l} p(T_l|T_{l-1}) p(T_{l-1}|T_{l-2}), \ldots, p(T_2|T_1) p(T_1)\, dT_{l-1}\ldots dT_2 dT_1 dT_l \\
&= \int_0^\infty\int_0^{T_l}\int_{T_1}^{T_l} \cdots \int_{T_{l-2}}^{T_l} e^{-aT_l} \Lambda^l e^{-\Lambda T_l}\, dT_{l-1}\ldots dT_2 dT_1 dT_l \\
&= \int_0^\infty\int_{T_1}^\infty\int_{T_2}^\infty, \ldots, \int_{T_{l-1}}^\infty e^{-aT_l} \Lambda^l e^{-\Lambda T_l}\, dT_l\ldots dT_3 dT_2 dT_1 \\
&= \int_0^\infty\int_{T_1}^\infty\int_{T_2}^\infty \cdots \int_{T_{l-2}}^\infty \frac{\Lambda^l}{\Lambda + a} e^{-(\Lambda+a)T_{l-1}}\, dT_{l-1}\ldots dT_3 dT_2 dT_1 \\
&\ \vdots \\
&= \frac{\Lambda^l}{(\Lambda + a)^l}, \qquad l = 1, 2, \ldots
\end{aligned}$$

Similarly

$$\mathbf{E}\{e^{-b\tau_{m,l}}\} = \frac{\lambda^m}{(\lambda+b)^m}$$
$$\mathbf{E}\left\{e^{-\frac{T_l}{\Gamma}}\right\} = \frac{\Lambda^l}{\left(\Lambda+\frac{1}{\Gamma}\right)^l}$$
$$\mathbf{E}\left\{e^{-\frac{\tau_{m,l}}{\gamma}}\right\} = \frac{\lambda^m}{\left(\lambda+\frac{1}{\gamma}\right)^m}$$

for $l = 0, 1, \ldots, L$ and $m = 0, 1, \ldots, M$. Hence

$$\begin{aligned}\mathrm{cor}\{H[k_1], H[k_2]\} &= e^{-j\frac{2\pi(\overline{k}_1-\overline{k}_2)m_0}{N}} \\ &\times \frac{\left(\sum_{l=0}^{L}\frac{\Lambda^l}{(\Lambda+a)^l}\right)\times\left(\sum_{m=0}^{M}\frac{\lambda^m}{(\lambda+b)^m}\right)}{\left(\sum_{l=0}^{L}\frac{\Lambda^l}{\left(\Lambda+\frac{1}{\Gamma}\}\right)^l}\right)\times\left(\sum_{m=0}^{M}\frac{\lambda^m}{\left(\lambda+\frac{1}{\gamma}\right)^m}\right)} \\ &= e^{-j\frac{2\pi(\overline{k}_1-\overline{k}_2)m_0}{N}} \times \frac{\frac{1-\frac{\Lambda^{L+1}}{(\Lambda+a)^{L+1}}}{1-\frac{\Lambda}{\Lambda+a}}\times\frac{1-\frac{\lambda^{M+1}}{(\lambda+b)^{M+1}}}{1-\frac{\lambda}{\lambda+b}}}{\frac{1-\frac{\Lambda^{L+1}}{(\Lambda+\frac{1}{\Gamma})^{L+1}}}{1-\frac{\Lambda}{\Lambda+\frac{1}{\Gamma}}}\times\frac{1-\frac{\lambda^{M+1}}{(\lambda+\frac{1}{\gamma})^{M+1}}}{1-\frac{\lambda}{\lambda+\frac{1}{\gamma}}}}.\end{aligned}$$

When L and M are large

$$\begin{aligned}\mathrm{cor}\{H[k_1], H[k_2]\} &\approx e^{-j\frac{2\pi(\overline{k}_1-\overline{k}_2)m_0}{N}} \\ &\times\frac{1+\frac{\Lambda\Gamma}{1+j\frac{2\pi(\overline{k}_1-\overline{k}_2)\Gamma}{NT_s}}}{1+\Lambda\Gamma}\times\frac{1+\frac{\lambda\gamma}{1+j\frac{2\pi(\overline{k}_1-\overline{k}_2)\gamma}{NT_s}}}{1+\lambda\gamma}\end{aligned}$$

and (11) follows.

Appendix C
Derivation of (24)

For the 1Tx2Rx scheme, it follows from (23) that

$$\begin{aligned}\widehat{x}[k] &= H_{11}^*[k]y_1[k] + H_{21}^*[k]y_2[k] \\ &= H_{11}^*[k]\left(H_{11}[k]x[k]+w_1[k]\right) + H_{21}^*[k] \\ &\quad\times\left(H_{21}[k]x[k]+w_2[k]\right) \\ &= \left(|H_{11}[k]|^2+|H_{21}[k]|^2\right)x[k] + H_{11}^*[k]w_1[k] \\ &\quad + H_{21}^*[k]w_2[k].\end{aligned}$$

Let E_b' denote the energy per bit in $x[k]$. Then

$$\begin{aligned}\mathrm{BER}_{\mathrm{uc}}^{1\mathrm{Tx}2\mathrm{Rx}} &= \mathbf{E}\left\{Q\left(\sqrt{\frac{2\left(|H_{11}[k]|^2+|H_{21}[k]|^2\right)E_b'}{N_0}}\right)\right\} \\ &= \mathbf{E}\left\{Q\left(\sqrt{\frac{2\left(|h_{11}[k]|^2+|h_{21}[k]|^2\right)E_b}{N_0}}\right)\right\} \\ &= \mathbf{E}\left\{Q\left(\sqrt{2\left(|h_{11}[k]|^2+|h_{21}[k]|^2\right)\mathrm{SNR}_r}\right)\right\}\end{aligned} \tag{31}$$

where $E_b = \mathbf{E}\{|H[k]|^2\} \times E_b'$ is the average received energy per bit per antenna, and $h_{11}[k]$ and $h_{21}[k]$ are statistically independent and circularly Gaussian distributed with $\mathbf{E}\{|h_{11}[k]|^2\} = \mathbf{E}\{|h_{21}[k]|^2\} = 1$. Similarly, we have

$$\mathrm{BER}_{\mathrm{uc}}^{2\mathrm{Tx}1\mathrm{Rx}} = \mathbf{E}\left\{Q\left(\sqrt{\left(|h_{11}[k]|^2+|h_{12}[k]|^2\right)\mathrm{SNR}_r}\right)\right\} \tag{32}$$

and (33), shown at the bottom of the page.

Here, $h_{lj}[k]$ are statistically independent and circularly Gaussian distributed with $\mathbf{E}\{|h_{lj}[k]|^2\} = 1$. Moreover, the sum $x = \sum_{l,j}|h_{lj}[k]|^2$ is chi-square distributed, with the probability density function given by

$$f(x) = \frac{1}{(K-1)!}x^{K-1}e^{-x} \tag{34}$$

where K is the number of $|h_{lj}[k]|^2$ terms in the sum, i.e., the chi-square distribution has $2K$ degrees of freedom. Taking the expectation of (31)–(33) with respect to (34) gives (24).

Appendix D
Derivation of (25)

From (34), $x = \sum_{l,j}|h_{lj}[k]|^2$ is chi-square distributed, and its cumulative distribution function is given by

$$\begin{aligned}F(x) &= \int_0^x f(\lambda)d\lambda = \int_0^x \frac{1}{(K-1)!}\lambda^{K-1}e^{-\lambda}d\lambda \\ &= 1 - \sum_{l=0}^{K-1}\frac{1}{l!}x^l e^{-x}\end{aligned}$$

from which we are able to see that the ninetieth-percentile cutoff gain $x_{K,90\%}$ satisfies

$$F(x_{K,90\%}) = 0.10. \tag{35}$$

$$\mathrm{BER}_{\mathrm{uc}}^{2\mathrm{T}\times2\mathrm{R}\times} = \mathbf{E}\left\{Q\left(\sqrt{\left(|h_{11}[k]|^2+|h_{12}[k]|^2+|h_{21}[k]|^2+|h_{22}[k]|^2\right)\mathrm{SNR}_r}\right)\right\} \tag{33}$$

For any given K, we can find a unique positive real number $x_{K,90\%}$ that satisfies (35). For $K = 2$ and $K = 4$, we get $x_{2,90\%} = 0.532$ and $x_{4,90\%} = 1.745$. For the 1Tx2Rx scheme, the uncoded BER for a given channel realization is

$$Q\left(\sqrt{2\left(|h_{11}[k]|^2 + |h_{21}[k]|^2\right)\mathrm{SNR}_r}\right).$$

Since the ninetieth-percentile cutoff gain is $x_{2,90\%}$, then we have

$$\mathrm{BER}_{\mathrm{uc},90\%}^{\mathrm{1Tx2Rx}} \approx Q\left(\sqrt{2x_{2,90\%}\mathrm{SNR}_r}\right) = Q\left(\sqrt{1.064\,\mathrm{SNR}_r}\right).$$

Consequently, (25) follows.

References

[1] Q. Zou, A. Tarighat, and A. H. Sayed, "Performance analysis and range improvement in multiband-OFDM UWB communications," in *Proc. IEEE ICASSP*, Toulouse, France, May 2006, pp. 629–632.

[2] I. Oppermann, M. Hämäläinen, and J. Iinatti, Eds., *UWB: Theory and Applications*. Hoboken, NJ: Wiley, 2004.

[3] M. Ghavami, L. Michael, and R. Kohno, *Ultra Wideband Signals and Systems in Communication Engineering*. Hoboken, NJ: Wiley, 2004.

[4] L. Yang and G. B. Giannakis, "Ultra-wideband communications: An idea whose time has come," *IEEE Signal Process. Mag.*, vol. 21, no. 6, pp. 26–54, Nov. 2004.

[5] "New public safety applications and broadband Internet access among uses envisioned by FCC authorization of ultra-wideband technology," *Revision of Part 15 of the Commission's Rules Regarding Ultra-Wideband Transmission Systems, Federal Communications Commission (FCC)*, Feb. 14, 2002, Washington, DC.

[6] *IEEE 802.15 wireless personal area networks (WPAN) high rate alternative PHY task group 3a (TG3a)*. [Online]. Available: http://www.ieee802.org/15/pub/TG3a.html

[7] A. Batra, J. Balakrishnan, G. R. Aiello, J. R. Foerster, and A. Dabak, "Design of a multiband OFDM system for realistic UWB channel environments," *IEEE Trans. Microw. Theory Tech.*, vol. 52, no. 9, pp. 2123–2138, Sep. 2004.

[8] *MultiBand OFDM physical layer specification*, 2005. MultiBand OFDM Alliance Special Interest Group.

[9] Y. Xin, Z. Wang, and G. B. Giannakis, "Space–time diversity systems based on linear constellation precoding," *IEEE Trans. Wireless Commun.*, vol. 2, no. 2, pp. 294–309, Mar. 2003.

[10] E. G. Larsson and P. Stoica, *Space–Time Block Coding for Wireless Communications*. New York: Cambridge Univ. Press, 2003.

[11] J. R. Foerster, M. Pendergrass, and A. F. Molisch, *A Channel Model for Ultrawideband Indoor Communication*, 2003. IEEE 802.15.3a standardization group.

[12] D. Tse and P. Viswanath, *Fundamentals of Wireless Communication*. New York: Cambridge Univ. Press, 2005.

[13] R. D. Wesel, "Convolutional codes," in *Wiley Encyclopedia of Telecommunications*, vol. 1, J. G. Proakis, Ed. Hoboken, NJ: Wiley, 2003, pp. 598–606.

[14] U. Fincke and M. Pohst, "Improved methods for calculating vectors of short length in a lattice, including a complexity analysis," *Math. Comput.*, vol. 44, no. 170, pp. 463–471, Apr. 1985.

[15] E. Viterbo and J. Boutros, "A universal lattice code decoder for fading channels," *IEEE Trans. Inf. Theory*, vol. 45, no. 5, pp. 1639–1642, Jul. 1999.

[16] A. H. Sayed, *Fundamentals of Adaptive Filtering*. Hoboken, NJ: Wiley, 2003.

[17] S. M. Alamouti, "A simple transmit diversity technique for wireless communications," *IEEE J. Sel. Areas Commun.*, vol. 16, no. 8, pp. 1451–1458, Oct. 1998.

Qiyue Zou (S'06) received the B.Eng. and M.Eng. degrees in electrical and electronic engineering from Nanyang Technological University (NTU), Singapore, in 2001 and 2004, respectively. He is currently working toward the Ph.D. degree at the Department of Electrical Engineering, University of California, Los Angeles.

From 2001 to 2004, he was with the Centre for Signal Processing, NTU, where he worked on statistical and array signal processing. His current research interests include signal processing, information theory, and wireless communications.

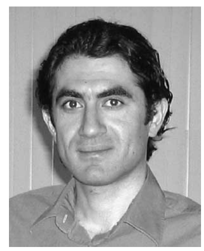

Alireza Tarighat (S'00–M'05) received the B.Sc. degree in electrical engineering from Sharif University of Technology, Tehran, Iran, in 1998 and the M.Sc. and Ph.D. degrees in electrical engineering from the University of California, Los Angeles (UCLA), in 2001 and 2005, respectively.

During the summer of 2000, he was with Broadcom, El Segundo, CA, where he worked on IEEE 802.11 transceivers. From 2001 to 2002, he was with Innovics Wireless, Los Angeles, where he worked on system and ASIC development of advanced antenna diversity and rake processing for 3G WCDMA mobile terminals. Since 2005, he has been with WiLinx, Los Angeles, working on system and silicon development of UWB wireless networks. His research interests are in communications theory and signal processing, including MIMO OFDM systems, multiuser MIMO wireless networks, algorithms for impairments compensation, and experimental and practical communications systems.

Dr. Tarighat was the recipient of the Gold Medal in the National Physics Olympiad, Iran, in 1993, the Honorable Mention Diploma in the 25th International Physics Olympiad, Beijing, China, in 1994, and the Outstanding Ph.D. Dissertation Award in Electrical Engineering from UCLA in 2006.

Ali H. Sayed (F'01) received the Ph.D. degree in electrical engineering from Stanford University, Stanford, CA, in 1992.

He is a Professor and the Chairman of the Department of Electrical Engineering, University of California, Los Angeles. He is also the Principal Investigator of the UCLA Adaptive Systems Laboratory (http://www.ee.ucla.edu/asl). He is the author or coauthor of over 270 papers published in international journals and conference proceedings, is the author of *Fundamentals of Adaptive Filtering* (New York: Wiley, 2003), and is the coauthor of the research monograph *Indefinite Quadratic Estimation and Control* (Philadelphia, PA: SIAM, 1999) and of the graduate-level textbook *Linear Estimation* (Englewood Cliffs, NJ: Prentice-Hall, 2000). He is also a coeditor of the volume *Fast Reliable Algorithms for Matrices with Structure* (Philadelphia, PA: SIAM, 1999). He has contributed several articles to engineering and mathematical encyclopedias and handbooks. His research interests span several areas, including adaptive and statistical signal processing, filtering and estimation theories, signal processing for communications, interplays between signal processing and control methodologies, system theory, and fast algorithms for large-scale problems.

Dr. Sayed is a member of the Signal Processing Theory and Methods Technical Committee and the Signal Processing for Communications Technical Committee, both of the IEEE Signal Processing Society. He was the Editor-in-Chief of the IEEE TRANSACTIONS ON SIGNAL PROCESSING during 2003–2005 and is now serving as the Editor-in-Chief of the *EURASIP Journal on Advances in Signal Processing*. He is serving as the General Chairman of the 2008 IEEE International Conference on Acoustics, Speech, and Signal Processing and is a member of the Board of Governors of the IEEE Signal Processing Society. He has served on the program committees of several international meetings. He was the recipient of the 1996 IEEE Donald G. Fink Award, the Best Paper Award from the IEEE Signal Processing Society in 2002, the Kuwait Prize in Basic Science in 2003, the Frederick E. Terman Award in 2005, a Young Author Best Paper Award in 2005 from the IEEE Signal Processing Society, and two Best Student Paper Awards at international meetings.